Journal of Luminescence 200 (2018) 14–18

Contents lists available at ScienceDirect

Journal of Luminescence

journal homepage: www.elsevier.com/locate/jlumin

A two-channel mechanism for the asymmetric excited-state intramolecular double proton transfer in a hydroxyflavone derivative

Qingchi Meng[a,c], Songqiu Yang[a,c], Guanghua Ren[a,c], Tianshu Chu[a,b,*]

[a] State Key Laboratory of Molecular Reaction Dynamics, Dalian Institute of Chemical Physics, Chinese Academy of Sciences, Dalian 116023, PR China
[b] Institute for Computational Sciences and Engineering, Laboratory of New Fiber Material and Modern Textile, the Growing Base for State Key Laboratory, Qingdao University, Qingdao 266071, PR China
[c] University of the Chinese Academy of Sciences, Beijing 100049, PR China

ARTICLE INFO

Keywords:
Excited-state double proton transfer
Hydroxyflavone fluorophore
DFT/TDDFT
Hydrogen bonding
Tautomerism
Fluorescence emission and quenching

ABSTRACT

The excited-state proton transfer (ESPT) mechanism of 3,7-dihydroxy-2-phenyl-6-acetyl-4H-chromen-4-one (DPACO) fluorophore was studied by the density functional theory (DFT) and time-dependent density functional theory (TD-DFT) with CAM-B3LYP functional and 6–31 + G(d,p) basis set. The computation levels are reliable as evidenced by the accordance between theory and experiment. In the ground state of DPACO, two intramolecular hydrogen bonds were formed. After photo-excitation, the electron density redistributions provide the driving force for hydrogen-bonding strengthening and ESPT. The constructed potential energy surfaces (PESs) along proton transfer (PT) coordinates indicate that two PT channels exist in the excited state. Among various PT tautomers, T4*is theoretically assigned as the main fluorescence emitter, while the low fluorescence quantum yield possibly correlate with the accelerated internal conversion pathway in the PT tautomer T6*.

1. Introduction

Excited state proton transfer (ESPT) reaction, one of the most elementary processes in chemistry and biology [1–10], has attracted tremendous attention since the first experimental observation of the phenomenon by Weller [11,12]. ESPT has been widely observed and applied in a variety of areas including organic light emitting devices [13–15], photoswitches [16], laser dyes [17], fluorescent sensors [18], drug delivery [19], etc. Systems undergoing ESPT usually comprise proton donor and acceptor groups in close proximity through intra- or intermolecular hydrogen bonds. Common proton donor can be hydroxyl or amino group while common proton acceptor can be carbonyl oxygen or pyridinyl nitrogen atom. Being a unique site-specific interaction, hydrogen bonding plays important role in excited-state dynamical processes of molecules [20]. Electronic excited-state hydrogen bonding should have effects on many photophysical or photochemical processes such as fluorescence quenching [21], photoinduced electron transfer [22] and ESPT [23,24], etc. Recently, Han and coworkers have provided new insight into the influence of hydrogen bonding on photodynamical processes in the electronic excited state [21,22,25–27]. On this account, many processes involving excited-state hydrogen bonding should be revisited.

Hydroxyflavone derivatives have important biological applications [28,29] and also serve as model molecules for ESPT researches [30–35]. Recently, Serdiuk and Roshal have synthesized a series of new hydroxyflavone derivatives, including 3,7-dihydroxy-2-phenyl-6-(3-phenylpropanoyl) − 4H-chromen-4-one (abbreviated as DPPCO), with the aim to investigate the excited-state intramolecular double proton transfer (ESIDPT) [30]. In this work, we truncated DPPCO to DPACO by substituting the phenylpropanoyl group with acetyl group for calculation cost consideration. Structures of all possible DPACO tautomers are shown in Fig. 1, where 'N' represents the normal form, 'T4' or 'T6' represents the tautomerization occurs approximate to carbon C4 or C6, and 'D' represents tautomerization occurs on both sites. Unless specifically stated, 'N*', 'T4*', 'T6*' and 'D*' represent corresponding stable structures in the excited state of S1. DPPCO (or DPACO for the truncated one) has two intramolecular hydrogen bonding sites and emits fluorescence with large stokes shift ($\Delta\nu$ = 10940 cm^{-1}), but the low fluorescence quantum yield suggests existence of an efficient dark deactivation pathway. Time-resolved fluorescence spectroscopy of DPPCO showed that there are two decay components with lifetimes of ~ 25 ps and 5.89 ns. It was experimentally proposed that the short decay component corresponds to T6* and the long decay component corresponds to D*. As pointed out by the original authors, the two proton transfer (PT) sites are asymmetric, and they excluded the possibility of emission from T4* base on their analysis of the steady-state and time-

* Corresponding author at: State Key Laboratory of Molecular Reaction Dynamics, Dalian Institute of Chemical Physics, Chinese Academy of Sciences, Dalian 116023, PR China.
E-mail addresses: tschu@dicp.ac.cn, tschu008@163.com (T. Chu).

https://doi.org/10.1016/j.jlumin.2018.03.095
Received 10 November 2017; Received in revised form 28 March 2018; Accepted 31 March 2018
Available online 02 April 2018
0022-2313/

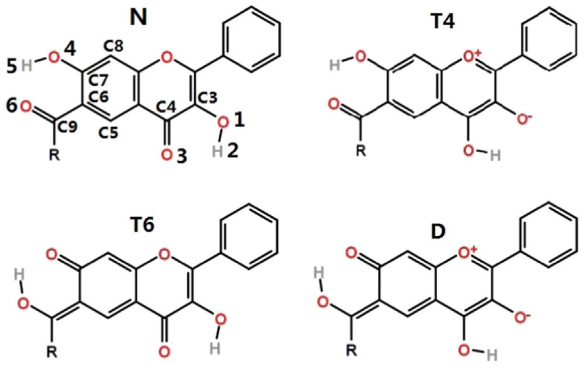

Fig. 1. Structures of DPACO (R = CH_3) and DPPCO (R = $(CH_2)_2Ph$) in N, T4, T6, and D forms. Also atomic numberings are labeled in N form structure.

resolved spectroscopy [30]. But is the PT process in O1-H2-O3 site really suppressed by that in O4-H5-O6 site? What is the relationship between the processes in the two PT sites? In order to get more insight into these ESPT processes, we carried out theoretical research on PT mechanism of DPACO fluorophore. All possible tautomers of DPACO in electronic ground and excited states have been optimized. Frontier molecular orbitals, Mulliken and NPA charge distribution, electronic vertical excited energies (EVEEs) were calculated. The 2-dimentional potential energy surfaces scanned along two PT coordinates as well as transition state optimization results indicate a two-channel ESIDPT mechanism, somewhat different from the experimental suggestion.

2. Theoretical method

All calculations were performed using Gaussian 16 program suite [36]. Density functional theory (DFT) [37] and time-dependent DFT (TD-DFT) [38] were used for ground-state and excited-state geometric optimizations as well as energy calculations. The TD-DFT method has been shown to be a very powerful tool to describe hydrogen bonding and PT reactions in the excited state [22,25,26,39–42]. Becke three-parameter hybrid exchange functional with Lee-Yang-Parr gradient-corrected correlation functional in Handy and coworker's long-range-corrected version, the CAM-B3LYP [43] functional was used with the 6–31 + G(d,p) basis set. All the optimized local minima and transition state geometries were confirmed by the vibrational frequency analysis. Methylcyclohexane was chosen as the solvent throughout our calculations. Linear response polarizable continuum model (LR-PCM) was used for EVEE calculations. Potential energy surfaces were relaxedly scanned along two generalized internal coordinates, PT1 and PT2, which are defined as PT1 = R(O1,H2)-R(H2,O3) and PT2 = R(O4,H5)-R(H5,O6). Potential energy curves were also relaxedly scanned along dihedral angle C5-C6-C9-O6. Atomic numberings are depicted in Fig. 1. The integral accuracy was 10^{-12} and DFT grid was ultrafine, as being the default settings in Gaussian 16.

Since relaxed scan of PES is very time-consuming, we have replaced the phenylpropanoyl group in DPPCO with the acetyl group in DPACO throughout our calculation. To confirm the rationality of such truncation, the EVEEs of DPPCO and DPACO have been listed and compared in supporting information (Table S1), which showed little difference as being within about 0.01 eV. Further, tautomers of DPACO have the same energy sequence with those of DPPCO (Table S2), which also proved the reliability of this treatment.

3. Results and discussion

3.1. Geometric structures

Key geometric parameters related to intramolecular hydrogen bonding were given in Table 1. All the optimized geometries were testified to be local minima by the absence of imaginary mode in vibrational frequency analysis. Note that T4, T6 and D tautomers have no corresponding optimized geometries in S0 while T4*, T6* and D* do have in the S1 state. Since O1, H2, O3 belong to a five-member ring while O4, H5, O6 belong to a six-member ring, the hydrogen bonging distance in (O1,H2,O3) is longer than that in (O4,H5,O6), as being 1.999 to 1.651 (Å) in N, 1.821 to 1.561 (Å) in N*, 2.024 to 1.578 (Å) in T4*, 1.869 to 1.574 (Å) in T6*, 1.967 to 1.451 (Å) in D*, respectively. Therefore, the closer proximity in six-member ring can make ESPT reaction in O4-H5-O6 site more feasible. N form was testified to be the most stable tautomer in the ground state. After photo-excited to N*, bond lengths of O1-H2 and O4-H5 elongate from 0.979 and 0.993 to 1.002 and 1.011 (Å), respectively. Bond lengths of O3…H2 and O6…H5 shorten from 1.999 and 1.651 to 1.821 and 1.561 (Å), respectively. The distances between (O1,O3) and (O4,O6) also shorten from 2.613 and 2.546 to 2.523 and 2.491 (Å), respectively. Meanwhile the bond angles of O1-H2…O3 and O4-H5…O6 increase from 118.6 and 147.8 to 124.2 and 150.4 (°), respectively. All these changes, as well as the vibrational frequency shifts shown in Fig. S1, indicate that the intramolecular hydrogen bonding of O1-H2…O3 and O4-H5…O6 are strengthened in N*compared to those in N. The alteration in equilibrium geometry can facilitate ESPT reaction. This strengthening is caused by photoinduced charge redistribution, which is also the driving force for ESPT. More details about charge distribution will be discussed in Section 3.2.

Table 1
Key geometric parameters of optimized DPACO tautomers in S0 and S1. Units of internuclear distance 'R' and bond angle 'Alpha' are in (Å) and (°), respectively.

	N	N *	T4 *	T6 *	D*
R(O1,H2)	0.979	1.002	2.024	0.9927	1.967
R(H2,O3)	1.999	1.821	0.980	1.869	0.984
R(O1,O3)	2.613	2.523	2.615	2.543	2.584
Alpha(O1,H2,O3)	118.6	124.2	116.7	122.4	118.4
R(O4,H5)	0.993	1.011	1.007	1.574	1.451
R(H5,O6)	1.651	1.561	1.578	1.011	1.044
R(O4,O6)	2.546	2.491	2.501	2.506	2.434
Alpha(O4,H5,O6)	147.8	150.4	149.8	150.8	154.1

3.2. Electronic spectra and charge distribution analysis

The EVEEs in optimized geometries were calculated and given in Table 2. For comparison, the experimental results are also shown. Calculated results show that two major absorption peaks, centered in 328 nm and 264 nm, originate from N-S0 to N-S1 and N-S0 to N-S5 electronic state transitions. This agrees well with experimental absorption peaks in 352 nm and 284 nm. N-S1 exhibits typical π-π*character, which is composed mainly (88.8%) of highest occupied molecular orbital (HOMO) to lowest unoccupied molecular orbital (LUMO) electronic excitation. As shown in Fig. 2, HOMO and LUMO exhibit significant charge redistribution character in O1, O3, O4 and O6 atoms. The Mulliken and NPA charge distributions in four ESPT-related oxygen atoms are given in Table 3. It can be seen that after photo-excitation, O1 loses more electron density than O4, meanwhile O3 acquires more electron density than O6, which indicates O1-H2-O3 site has more potential to undergo ESPT reaction.

Emission data were obtained by calculating the EVEEs of DPACO tautomers optimized in S1 with LR-PCM method and were shown in Table 2. The calculated emission peaks originated from the four tautomers are quite different. The emission peaks shift to red in sequence of N*(384 nm), T6*(461 nm), T4*(554 nm) and D*(677 nm). Emission peak from T4*agrees best with the major fluorescence peak (562 nm) detected experimentally in Ref. [30]. As for emissions from other tautomers, no noticeable peak can be observed in the experimental steady-state emission spectra.

Table 2
Calculated absorption and emission EVEEs in different form of tautomers with corresponding state numbering (NO.), molecular orbital (MO) composition and oscillator strengths (ƒ). Also experimental steady-state absorption and emission peak wavelengths (λ), relative intensity (I_{rel}) of the two absorption peaks, deactivation lifetimes (τ) and corresponding fractional contributions (Per) detected at 560 nm [30] are presented for comparison. The calculated EVEEs and experimental spectra peaks are in unit (nm).

	Cal. Result					Exp. Result		
	Form	NO.	MO Composition	EVEEs	ƒ	λ	I_{rel}	τ / Per
Abs.	N	S1	HOMO→LUMO, (88.8%) HOMO→LUMO + 1, (5.8%)	328	0.56	352	0.51	———
		S5	HOMO-3→LUMO, (20.9%) HOMO-1→LUMO, (13.0%) HOMO→LUMO, (3.4%) HOMO→LUMO + 1, (53.2%)	264	0.75	284	1	———
Em.	N*	S1	HOMO→LUMO, (93.4%) HOMO→LUMO + 1, (3.6%)	384	0.58	562	———	25 ps/ 6%
	T4*	S1	HOMO→LUMO, (98.5%)	554	0.47			
	T6*	S1	HOMO→LUMO, (88.9%) HOMO-1→LUMO, (9.2%)	461	0.27			5.89 ns / 94%
	D*	S1	HOMO→LUMO, (98.4%)	677	0.35			

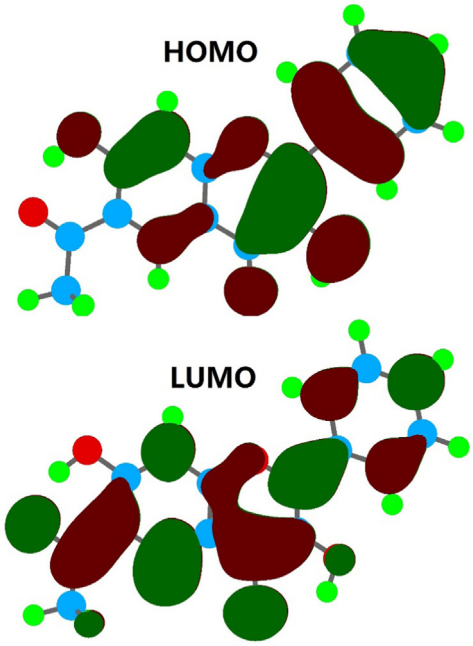

Fig. 2. Frontier molecular orbitals of DPPCO in N form geometry.

3.3. Potential energy surfaces (PESs)

To further explore the details about the PT mechanism, we scanned 2-dimentianal potential energy surfaces of both ground state (GS-PES) and excited state (ES-PES). The two coordinates are described in the theoretical method section. As shown in Fig. 3, T4*has the lowest energy comparing to the other three excited state tautomers. ES-PES shows that two PT channels exist to generate the most stable T4 * tautomer. That is, channel-a (through N * →T4 * , depicted by the red arrow in ES-PES) and channel-b (through T6 * →D*→T4 * , depicted by the purple arrows in ES-PES). By emitting a photon, T4 * deactivates to T4 (depicted by the left hollow arrow), then transforms to the stable N form through a ground state proton transfer (GSPT) process (depicted by the red arrow in GS-PES). In order to get the accurate barrier height, all transition states in channel-a and channel-b were optimized and thermal corrections to Gibbs free energies were added to the electronic energies. As shown in Fig. 4, TS-a is 0.57 kcal/mol higher than N * ; in channel-b, T6 * is 2.02 kcal/mol lower than N * ; transformation N * →T6 * is barrierless; and 2.23 kcal/mol is needed for T6 * to overcome the energy barrier of TS-b2. The tautomer D* is 2.02 kcal/mol higher than T4 * , and D*→T4 * transformation is also barrierless. Thus, T6 * may be assigned as the metastable intermediate species.

In Ref. [30], researchers also synthesized two other fluorophores 1b and 1c, which are similar to DPPCO. In fluorophore 1b, O1-H2 is substituted by hydrogen atom and thus the ESPT in O1-H2-O3 site is prohibited while that in O4-H5-O6 site can occur. In fluorophore 1c, H5 is substituted by methyl group and the ESPT in O4-H5-O6 is prohibited while the ESPT in O1-H2-O3 can happen as usual. The steady-state fluorescence spectra of 1c have almost identical shape and position with those of neutral DPPCO solution at 298 K, but two aspects are quite different. First, fluorophore 1c possesses normal emission at 77 K while DPPCO does not. Second, DPPCO suffers a one-hundred-time quantum yield loss comparing to fluorophore 1c, as being 0.11% to 11.6%. The original authors of the experimental paper deduced the conclusion of "DPPCO does not exist in T4 * form (in neutral solution)" with the reason like "the basic difference in the spectral behavior of 1a (e.g., DPPCO in the present paper) and 1c such as much lower fluorescence quantum yield, absence of the N * emission at 77 K in the case of 1a". In our opinion, the logic seems not so convinced. According to our calculation, the phenomenon that DPPCO shows no normal emission at 77 K may be the consequence of the fast transformation N * →T6 * that leads to the absence of N * . On the other hand, the fluorescence quenching or the low quantum yield of DPPCO is likely to be originated from its intermediate species. It is obvious that PT site O1-H2-O3 is rigid while O4-H5-O6 is rotatable. Previous studies have shown that

Table 3
Mulliken and NPA charge distributions in S0 and S1 as well as charge differences between the two states in N form structure.

	Mulliken				NPA			
	O1	O3	O4	O6	O1	O3	O4	O6
N-S0	− 0.603	− 0.639	− 0.557	− 0.512	− 0.722	− 0.651	− 0.718	− 0.620
N-S1	− 0.523	− 0.703	− 0.539	− 0.545	− 0.650	− 0.704	− 0.698	− 0.648
Difference	0.080	− 0.064	0.018	− 0.033	0.072	− 0.053	0.02	− 0.028

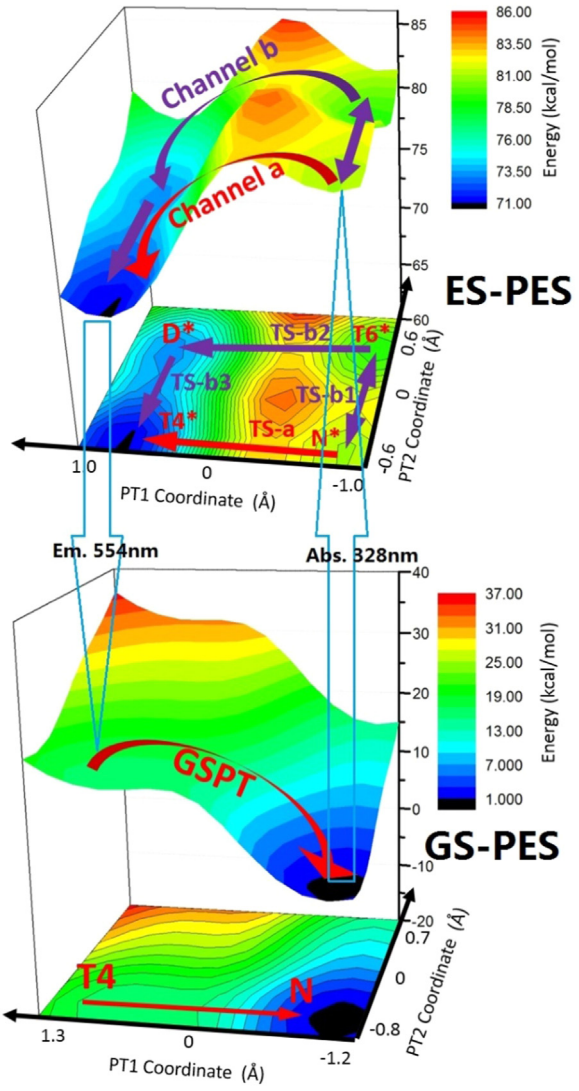

Fig. 3. 2-dimensional PESs of DPACO in ground state and excited state. The hollow arrows represent absorption and emission process, the red solid arrows and purple solid arrows in ES-PES represent two different PT channels in the excited state.

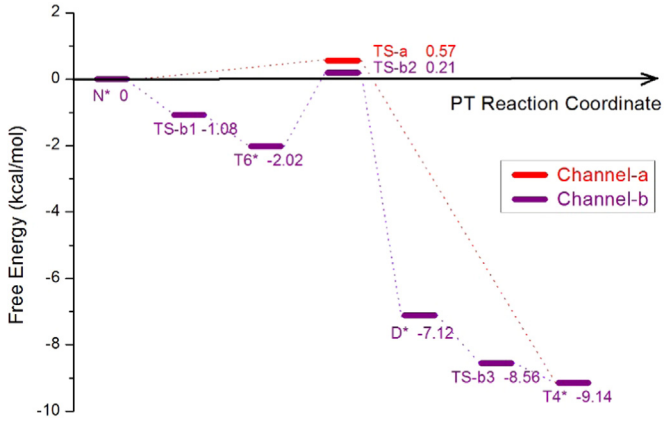

Fig. 4. Gibbs Free Energies in channel-a and channel-b. Here we use the excited-state energy of N * as reference.

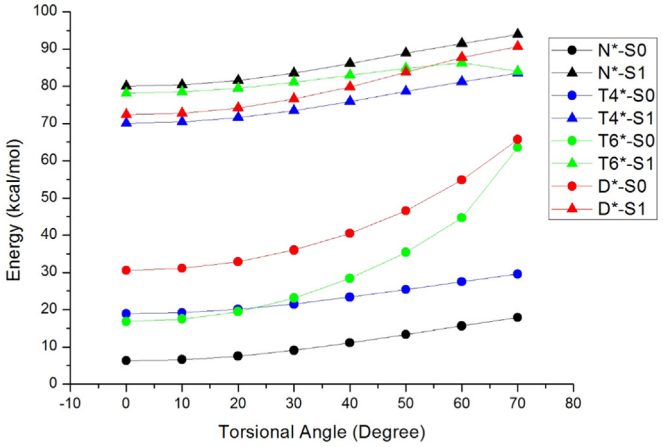

Fig. 5. Potential energy curves along the dihedral angle C5-C6-C9-O6 of the four excited-state tautomers.

torsional modes of rotation between PT donor and PT acceptor groups can decrease the quantum yield of the fluorophores [44]. This might provide a good explanation for why the quantum yield of 1b (1.0%) is ten times lower than that of 1c (11.6%) since PT site in 1b is rotatable while PT site in 1c is rigid. Here, we tentatively searched the non-radiative channel of DPPCO by scanning the potential energy curves along the dihedral angle C5-C6-C9-O6 of the four excited state tautomers. Of course, we note here that TD-DFT is not suitable for locating the conical intersection between multiple electronic states, and more accurate results should be obtained from the spin-flip (SF)-TD-DFT calculation [45] which is beyond the scope of the present study. Therefore, the TD-DFT curves we showed here only roughly reflect the energy trend with the torsion motion. As shown in Fig. 5, when H5 is covalently bonding with O6 (i.e. T6 * and D*), torsion along the dihedral angle C5-C6-C9-O6 would decrease the energy gap between S0 and S1. But this decrease does not happen when H5 is covalently bonding with O4 (i.e. N * and T4 *). According to the energy gap law [46], this torsion of intermediate species T6 * possibly provides an efficient internal conversion (IC) pathway between S0 and S1. In addition, from the experiment, it is known that the lifetime of fluorophores 1b and 1c is 0.473 ns and 2.19 ns, respectively; and the decay time of the long component of DPPCO is 5.89 ns, even longer than that of fluorophore 1c. Due to the possible existence of the fast IC pathway, tautomers that are H5-O6 covalently bonded (i.e. T6 * and D*) might have short lifetime like the case of fluorophore 1b while the tautomer T4 * without the fast decay pathway might have long lifetime like the case of fluorophore 1c. These lifetime values also imply that the final emitting species of DPPCO might be T4 * , not T6 * or D*.

Up to now, we can get the whole dynamics picture for ESPT in DPACO (or DPPCO). After photo-excitation, the majority species N * would quickly transform to T6 * . Considering the excess vibrational energy, N * →T4 * and T6 * →N * are also possible. In T6 * geometry, torsional mode of rotation along the dihedral angle C5-C6-C9-O6 possibly opens an efficient non-radiative pathway through IC between S1 and S0, which should be suppressed under cooling. This non-radiative process seems to correspond to the ~ 25 ps decay component within the vibrational relaxation time-scale. T4 * can be generated either through (T6 * →)N * →T4 * or T6 * →D* →T4 * . This theoretical picture is in consistent with experimental observation of DPPCO such as no emission of N * at both 298 K and 77 K, existence of an intermediate species, existence of an efficient dark deactivation pathway for the intermediate species, long living lifetime (~ 5 ns) for the fluorescent tautomer [30]. But, here, the theory tends to predict a different assignment for the fluorescent tautomer and a different dark deactivation pathway. That is, different from the experimental viewpoint that the fluorescence comes from D* and that the dark deactivation pathway is ESPT of

T6 * →D* , the present theory proposes that the fluorescence possibly comes from T4 * and that the ESPT process of T6 * →D* itself might not result in fluorescence quenching, but the geometry change of O4-H5-O6 PT site might open a non-radiative channel.

Furthermore, we would like to discuss about the different roles played by the two asymmetric PT sites and provide some suggestions that may improve the performance of this fluorophore. In the present case, O1-H2-O3 has higher PT potential than O4-H5-O6, but it has lower feasibility. As is well-known, PT potential is related to the energy difference between PT reactant and product while PT feasibility is related to the energy barrier and PT distance. Both factors can have impact on fluorescence of DPPCO. Here, we tentatively propose that a rigid structure fixing the dihedral angle C5-C6-C9-O6 might enhance the fluorescence quantum yield. Besides, a fine tuning of PT driving force in O4-H5-O6 site may invert the energy sequence of T4 * and D* tautomer. When D* becomes the most stable tautomer in the excited state, an even larger stokes shift can be expected. Further researches are under investigating.

4. Conclusion

In the present work, we have carried out a detailed theoretical study on ESPT reaction of the DPACO fluorophore. DFT and TD-DFT have been used for geometry optimization and energy calculation at the CAM-B3LYP/6–31 + G(d,p) level throughout. Optimized geometries and calculated frequencies indicate that intramolecular hydrogen bonds O1-H2…O3 and O4-H5…O6 are strengthened when the N form of DPACO is excited from S0 to S1. This strengthening would facilitate the ESPT reaction. It is suggested that the two major absorption peaks correspond to N-S0→N-S1 and N-S0→N-S5 excitation and the major fluorescence peak originates from T4 * tautomer, which is formed through two competing channels as the result of the asymmetric nature of the two PT sites. The fluorescence quenching might be caused by the torsion of the intermediate species T6 * . The present theoretical work partially agrees with the mechanism proposed experimentally, and presents a new possibility of the emitting species and non-radiative deactivation pathway. It is hoped that this paper may provide some useful information for ESPT fluorophore design.

Acknowledgments

This work is supported by the National Natural Science Foundation of China (Grant No. 21273234), the National Basic Research Program of China (Grant No. 2013CB834604) and the Open Fund of the State Key Laboratory of Molecular Reaction Dynamics in DICP, CAS (SKLMRD-K201817).

Appendix A. Supporting information

Supplementary data associated with this article can be found in the online version at http://dx.doi.org/10.1016/j.jlumin.2018.03.095.

References

[1] S.R. Meech, Chem. Soc. Rev. 38 (2009) 2922.
[2] S. Hammes-Schiffer, A.A. Stuchebrukhov, Chem. Rev. 110 (2010) 6939.
[3] H. Petek, J. Zhao, Chem. Rev. 110 (2010) 7082.
[4] O.A. Sytina, D.J. Heyes, C.N. Hunter, M.T. Alexandre, I.H.M. van Stokkum, R. van Grondelle, M.L. Groot, Nature 456 (2008) 1001.
[5] G.L. Cui, Z.G. Lan, W. Thiel, J. Am. Chem. Soc. 134 (2012) 1662.
[6] S.H. Xia, B.B. Xie, Q. Fang, G.L. Cui, W. Thiel, Phys. Chem. Chem. Phys. 17 (2015) 9687.
[7] Y. Houari, A. Charaf-Eddin, A.D. Laurent, J. Massue, R. Ziessel, G. Ulrich, D. Jacquemin, Phys. Chem. Chem. Phys. 16 (2014) 1319.
[8] C. Azarias, S. Budzak, A.D. Laurent, G. Ulrich, D. Jacquemin, Chem. Sci. 7 (2016) 3763.
[9] M. Savarese, E. Bremond, L. Antonov, I. Ciofini, C. Adamo, ChemPhysChem 16 (2015) 3966.
[10] L. Wilbraham, M. Savarese, N. Rega, C. Adamo, I. Ciofini, J. Phys. Chem. B 119 (2015) 2459.
[11] A. Weller, Z. Elektrochem. 60 (1956) 1144.
[12] H. Beens, Kh Grellman, M. Gurr, A.H. Weller, Discuss. Faraday Soc. (1965) 183.
[13] K. Kanosue, T. Shimosaka, J. Wakita, S. Ando, Macromolecules 48 (2015) 1777.
[14] S. Kim, J. Seo, H.K. Jung, J.J. Kim, S.Y. Park, Adv. Mater. 17 (2005) 2077.
[15] H. Roohi, F. Hejazi, N. Mohtamedifar, M. Jahantab, Spectrochim. Acta Part A 118 (2014) 228.
[16] S.J. Lim, J. Seo, S.Y. Park, J. Am. Chem. Soc. 128 (2006) 14542.
[17] K. Sakai, T. Tsuzuki, Y. Itoh, M. Ichikawa, Y. Taniguchi, Appl. Phys. Lett. 86 (2005) 3.
[18] J.Z. Zhao, S.M. Ji, Y.H. Chen, H.M. Guo, P. Yang, Phys. Chem. Chem. Phys. 14 (2012) 8803.
[19] S. Barman, S.K. Mukhopadhyay, M. Gangopadhyay, S. Biswas, S. Dey, N.D.P. Singh, J. Mat. Chem. B 3 (2015) 3490.
[20] T.S. Chu, B.T. Liu, Int. Rev. Phys. Chem. 35 (2016) 187.
[21] G.J. Zhao, K.L. Han, J. Phys. Chem. A 111 (2007) 9218.
[22] G.J. Zhao, J.Y. Liu, L.C. Zhou, K.L. Han, J. Phys. Chem. B 111 (2007) 8940.
[23] S. Chai, G.J. Zhao, P. Song, S.Q. Yang, J.Y. Liu, K.L. Han, Phys. Chem. Chem. Phys. 11 (2009) 4385.
[24] J.F. Zhao, H.B. Yao, J.Y. Liu, M.R. Hoffmann, J. Phys. Chem. A 119 (2015) 681.
[25] G.J. Zhao, K.L. Han, Acc. Chem. Res. 45 (2012) 404.
[26] G.J. Zhao, K.L. Han, ChemPhysChem 9 (2008) 1842.
[27] G.J. Zhao, K.L. Han, J. Phys. Chem. A 111 (2007) 2469.
[28] M. Samsonowicz, E. Regulska, M. Kalinowska, Chem. -Biol. Interact. 273 (2017) 245.
[29] X.D. Wang, J. Han, A. Chou, J.C. Yang, J.X. Pan, C.H. Borchers, Anal. Chem. 85 (2013) 7566.
[30] I.E. Serdiuk, A.D. Roshal, RSC Adv. 5 (2015) 102191.
[31] D. Ghosh, G. Ahamed, S. Batuta, N.A. Begum, D. Mandal, J. Phys. Chem. A 120 (2016) 44.
[32] K. Furukawa, N. Yamamoto, K. Hino, H. Sekiya, Phys. Chem. Chem. Phys. 18 (2016) 28564.
[33] P.T. Chou, S.C. Pu, Y.M. Cheng, W.S. Yu, Y.C. Yu, F.T. Hung, W.P. Hu, J. Phys. Chem. A 109 (2005) 3777.
[34] A.S. Klymchenko, A.P. Demchenko, New J. Chem. 28 (2004) 687.
[35] P.T. Chou, W.S. Yu, Y.M. Cheng, S.C. Pu, Y.C. Yu, Y.C. Lin, C.H. Huang, C.T. Chen, J. Phys. Chem. A 108 (2004) 6487.
[36] G.W.T.M.J. Frisch, H.B. Schlegel, G.E. Scuseria, M.A. Robb, J.R. Cheeseman, G. Scalmani, V. Barone, G.A. Petersson, H. Nakatsuji, X. Li, M. Caricato, A.V. Marenich, J. Bloino, B.G. Janesko, R. Gomperts, B. Mennucci, H.P. Hratchian, J.V. Ortiz, A.F. Izmaylov, J.L. Sonnenberg, D. Williams-Young, F. Ding, F. Lipparini, F. Egidi, J. Goings, B. Peng, A. Petrone, T. Henderson, D. Ranasinghe, V.G. Zakrzewski, J. Gao, N. Rega, G. Zheng, W. Liang, M. Hada, M. Ehara, K. Toyota, R. Fukuda, J. Hasegawa, M. Ishida, T. Nakajima, Y. Honda, O. Kitao, H. Nakai, T. Vreven, K. Throssell, J.A. Montgomery Jr., J.E. Peralta, F. Ogliaro, M.J. Bearpark, J.J. Heyd, E.N. Brothers, K.N. Kudin, V.N. Staroverov, T.A. Keith, R. Kobayashi, J. Normand, K. Raghavachari, A.P. Rendell, J.C. Burant, S.S. Iyengar, J. Tomasi, M. Cossi, J.M. Millam, M. Klene, C. Adamo, R. Cammi, J.W. Ochterski, R.L. Martin, K. Morokuma, O. Farkas, J.B. Foresman, D.J. Fox, Gaussian 16, Revision A.03, Gaussian, Inc., Wallingford CT, 2016.
[37] W. Kohn, A.D. Becke, R.G. Parr, J. Phys. Chem. 100 (1996) 12974.
[38] M.A.L. Marques, E.K.U. Gross, Annu. Rev. Phys. Chem. 55 (2004) 427.
[39] G.J. Zhao, K.L. Han, J. Comput. Chem. 29 (2008) 2010.
[40] N. Kungwan, F. Plasser, A.J.A. Aquino, M. Barbatti, P. Wolschann, H. Lischka, Phys. Chem. Chem. Phys. 14 (2012) 9016.
[41] B.K. Paul, N. Guchhait, J. Lumin. 131 (2011) 1918.
[42] G.H. Fan, K.L. Han, G.Z. He, Chin. J. Chem. Phys. 26 (2013) 635.
[43] T. Yanai, D.P. Tew, N.C. Handy, Chem. Phys. Lett. 393 (2004) 51.
[44] K. Skonieczny, J. Yoo, J.M. Larsen, E.M. Espinoza, M. Barbasiewicz, V.I. Vullev, C.H. Lee, D.T. Gryko, Chem. Eur. J. 22 (2016) 7485.
[45] Y.H. Shao, M. Head-Gordon, A.I. Krylov, J. Chem. Phys. 118 (2003) 4807.
[46] R. Englman, J. Jortner, Mol. Phys. 18 (1970) 145.